Comparing Type I and Type II Codebooks in 5G MIMO with Imperfect CSI at the Receiver

Hybrid Precoding Algorithms for Non Terrestrial Networks

Deyu Kong*, Giorgio Taricco†, Qing Guo*
* Harbin Institute of Technology, China
† Politecnico di Torino, Italy
E-mail: giorgio.taricco@polito.it

***Abstract*—This paper presents an energy-efficient downlink framework for single-satellite LEO systems, addressing challenges from limited power and satellite mobility. A hybrid analog–digital beamforming (HBF) architecture with a fully connected phased array is proposed to reduce RF chain usage while supporting multi-user coverage. The beamforming is optimized for energy efficiency under practical hardware constraints. A digital beamforming benchmark is first derived using fractional programming, followed by a hybrid algorithm based on alternating and manifold optimization with phase quantization. Simulations show notable energy gains over other schemes from the literature, confirming HBF's promise for next-generation Non-Terrestrial Networks (NTN).**

***Index Terms*—Non Terrestrial Networks (NTN), Hybrid analog–digital BeamForming (HBF), Energy Efficiency (EE).**

I. Introduction

LEO satellite constellations are key to future Non-Terrestrial Networks (NTNs), enabling services from remote emergency response to global broadband. Compared to GEO systems, LEO offers lower latency and better link budgets due to its lower altitude [1, 2, 3]. However, high orbital velocity causes fast channel variation and Doppler shifts, challenging multi-user reliability [4, 5]. Limited payload and power constrain complex or power-hungry methods, emphasizing energy-efficient resource use [6]. As NTNs grow in B5G/6G, efficient precoding is essential to manage power and interference [7, 8]. Though both uplink and downlink are vital, the downlink receives more attention due to its key role in high-data-rate broadband and multimedia services. Due to limited power and simple antennas, ground terminals struggle with uplink multi-antenna techniques. In contrast, a multi-antenna LEO satellite can form multiple downlink beams, boosting spectral efficiency for many users [9]. This high demand and power constraint call for advanced beamforming to optimize coverage, throughput, and energy efficiency.

Full digital beamforming (DBF) offers optimal control and interference management [10], but is impractical for LEO satellites due to high hardware, power, and complexity demands [11, 12]. Hybrid beamforming (HBF) is a more feasible alternative, splitting precoding between digital baseband and analog RF stages using phase shifters or amplifiers [13]. However, it faces challenges like phase quantization loss, amplifier nonlinearity, and complex real-time beam tracking [14, 15]. Early HBF research focused on mmWave and terahertz systems, where fully digital beamforming was limited by bandwidth and cost [16, 17]. Later studies showed that combining analog and digital precoding can closely match DBF performance with lower complexity [18]. These insights led to applying HBF in satellite systems, but LEO-specific challenges emerged, such as wide coverage, inter-beam interference, and dynamic channels [19, 20]. Solutions range from heuristics to joint analog–digital optimization, but higher phase-shifter resolution increases power and heat. Efficient, low-complexity algorithms are also needed for onboard autonomy [21, 22, 23, 24].

This paper presents a novel hybrid analog–digital precoding framework for single-satellite downlink, aiming to maximize energy efficiency under practical hardware constraints. Unlike methods assuming perfect CSI or focusing solely on throughput, our approach uses finite-resolution phase shifters and statistical CSI. We introduce a low-complexity algorithm combining fractional programming, quadratic transform, and alternating manifold optimization to handle non-convexity and discrete constraints. Simulations across various scenarios show our method outperforms conventional digital and hybrid beamforming in energy efficiency and interference management.

II. Downlink Transmission Model

This section summarizes the key aspects of the downlink transmission model, including the description of the hybrid beamforming structures and the characteristics of the channel equations modeling the system.

A. Hybrid Beamforming

Hybrid beamforming (HBF) combines digital and analog precoding to balance performance and hardware efficiency. By splitting precoding into a digital baseband and an analog RF stage (using phase shifters or amplifiers), HBF reduces RF chain requirements, lowering cost and power consumption. HBF can be implemented in two configurations: fully connected, where each RF chain connects to all antenna elements, and partially connected, where each RF chain is linked to a subset of antennas. These configurations are illustrated in Figs. 1 and 2, respectively.

The number of RF chains is significantly smaller than the number of antenna elements, thus reducing hardware complexity and digital beamforming dimensions. Though the partially connected design simplifies the layout and lowers implementation costs, it also introduces challenges such as

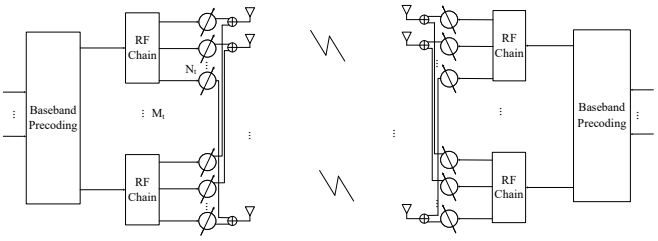

Fig. 1. Fully Connected HBF Architecture.

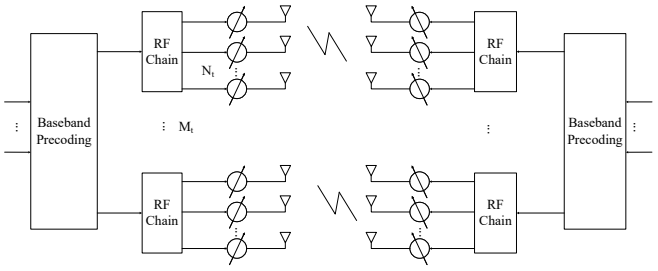

Fig. 2. Partially Connected HBF Architecture.

more complex signal modeling and wider beamwidths due to fewer antennas per sub-array, leading to reduced array gain and a more diffuse beam pattern. For LEO satellite systems, balancing hardware complexity and data-rate performance is critical. Thus, this section focuses on fully connected hybrid beamforming architectures [25].

B. System Model

The system is modeled as a single-satellite LEO downlink, where one satellite provides service to multiple single-antenna users within its coverage area, which is the 3-dB satellite footprint described in [26]. As depicted in Fig. 3, the antenna elements on the satellite are arranged in a planar array, spaced half a wavelength apart from each other. We assume a nadir-pointing satellite antenna. Users have known distances from

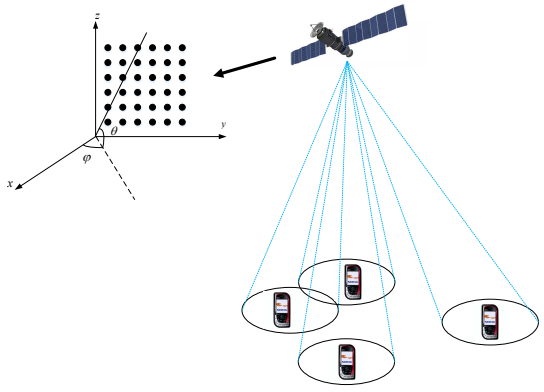

Fig. 3. Schematic Diagram of Multi-beam Downlink Transmission of a Single LEO Satellite.

the satellite (available via the GNSS-aided beacon uplink) and the channel gains between the satellite and different users are uncorrelated [27]. Let the total number of users be K and let the user index be $k = 1, \ldots, K$. Denote the channel matrix at time t and frequency f from the N_t satellite antenna elements to the single k-th user antenna by $\boldsymbol{h}_k(t, f)$. The channel matrix can be written as

$$\boldsymbol{h}_k(t, f) = \boldsymbol{v}_k g_k(t, f)^*. \tag{1}$$

where

$$\boldsymbol{v}_k = \Big(e^{-j2\pi(z_1 \sin(\theta_{k,1}) + y_1 \cos(\theta_{k,1}) \sin(\varphi_{k,1}))/\lambda}, \ldots, e^{-j2\pi(z_{N_\mathrm{t}} \sin(\theta_{k,N_\mathrm{t}}) + y_{N_\mathrm{t}} \cos(\theta_{k,N_\mathrm{t}}) \sin(\varphi_{k,N_\mathrm{t}}))/\lambda}\Big)^H \tag{2}$$

The vector $\boldsymbol{v}_k \in \mathbb{C}^{N\mathrm{t}\times 1}$, defined in (2), represents the column steering vector of the planar array and remains unaffected by individual multipath components due to the large satellite distance. The coordinates (y_i, z_i) specify the position of the i-th antenna element within the planar array, as illustrated in Fig. 3, while the angles $\theta_{k,i} \in (-\pi/2, \pi/2)$ and $\varphi_{k,i} \in [0, 2\pi)$ correspond to the elevation and azimuth of each antenna element, respectively. The scalar $g_k(t, f)$ denotes the time–frequency-dependent channel gain between the satellite and the k-th user, expressed as

$$g_k(t, f) = \sum_{p=1}^{P_k} \alpha_{k,p} \cdot \exp j2\pi(t\delta_{k,p} - f\tau_{k,p}), \tag{3}$$

where P_k is the number of multipath components, and $\alpha_{k,p}$, $\delta_{k,p}$, and $\tau_{k,p}$ represent the complex gain, Doppler shift, and propagation delay of the p-th path to the k-th user. Applying the Central Limit Theorem (CLT), we get the approximation:

$$g_k(t, f) \sim \mathcal{CN}\left(\sqrt{\frac{\beta_k \gamma_k}{\beta_k + 1}}, \frac{\gamma_k}{\beta_k + 1}\right). \tag{4}$$

The transmitted signal vector is denoted by

$$\boldsymbol{x}(t, f) = \sum_{k=1}^{K} \boldsymbol{b}_k s_k(t, f). \tag{5}$$

Here, $\boldsymbol{b}_k \in \mathbb{C}^{N_\mathrm{t}\times 1}$ is the beamforming vector for the k-th user. As a consequence, $\boldsymbol{x}(t, f) \in \mathbb{C}^{N_\mathrm{t}\times 1}$, too. Dropping the dependence on the time-frequency variables (t, f), the received signal for the k-th user is:

$$\begin{aligned} y_k &= \boldsymbol{h}_k^H \boldsymbol{x} + n_k \\ &= \boldsymbol{h}_k^H \boldsymbol{b}_k s_k + \boldsymbol{h}_k^H \sum_{i \neq k} \boldsymbol{b}_i s_i + n_k. \end{aligned} \tag{6}$$

Here, $n_k \sim \mathcal{CN}(0, N_0)$ is the circularly-symmetric zero-mean complex Gaussian random variable characterizing the noise component for the k-th user, and s_k is the symbol transmitted by the k-th user. We assume that $\mathbb{E}[|s_k|^2] = 1$. For the fully connected HBF architecture, the beamforming vectors are $\boldsymbol{b}_k = \boldsymbol{V}\boldsymbol{w}_k$, where $\boldsymbol{V} \triangleq (\boldsymbol{v}_1, \ldots, \boldsymbol{v}_{M_\mathrm{t}}) \in \mathbb{C}^{N_\mathrm{t}\times M_\mathrm{t}}$ represents the RF *analog* beamforming matrix characterizing the RF network and $\boldsymbol{w}_k \in \mathbb{C}^{M_\mathrm{t}\times 1}$ represents the *digital* baseband

beamforming vector for the k-th user. The number of RF chains M_{t} satisfies the inequalities: $K \leq M_{\mathsf{t}} \leq N_{\mathsf{t}}$. The RF architecture includes mixers, local oscillators, low-pass filters, baseband amplifiers, and power amplifiers.

The first step in signal transmission is baseband processing. Let $\boldsymbol{s} \triangleq (s_1, s_2, \ldots, s_K)^T \in \mathbb{C}^{K\times 1}$ represent the digital baseband transmit symbols, and let $\mathbb{E}\{\boldsymbol{s}\boldsymbol{s}^H\} = \boldsymbol{I}_K$. After processing the signal vector $\boldsymbol{s}$ by the digital beamforming matrix $\boldsymbol{W} \triangleq (\boldsymbol{w}_1, \boldsymbol{w}_2, \ldots, \boldsymbol{w}_K) \in \mathbb{C}^{M_{\mathsf{t}}\times K}$, the resulting baseband signal vector becomes $\boldsymbol{u} \triangleq \boldsymbol{W}\boldsymbol{s}, \boldsymbol{u} = (u_1, u_2, \ldots, u_{M_{\mathsf{t}}})^T \in \mathbb{C}^{M_{\mathsf{t}}\times 1}$. The baseband signal is upconverted to RF, processed by the analog beamforming matrix $\boldsymbol{V}$, and transmitted via antenna elements. With limited b-bit phase shifter resolution, phase angles are constrained to steps of $\Delta = 2\pi/2^b$, so that $\boldsymbol{V} \in \mathcal{S}_b^{N_{\mathsf{t}}\times M_{\mathsf{t}}}$, where $\mathcal{S}_b = \{\omega, \omega^2, \ldots, \omega^{2^b}\}$ and $\omega = e^{j\Delta}$. The case $b \to \infty$ denotes the *fully-digital* scenario. The downlink SINR for the k-th user is given by

$$\mathrm{SINR}_k \triangleq \frac{|\boldsymbol{h}_k^H \boldsymbol{b}_k|^2}{\sum_{\ell\neq k} |\boldsymbol{h}_k^H \boldsymbol{b}_\ell|^2 + N_0}. \tag{7}$$

Due to challenges in obtaining instantaneous CSI (iCSI) in LEO systems, statistical CSI (sCSI) is used, with the average rate for user k defined as $R_k = \mathbb{E}[\log_2(1 + \mathrm{SINR}_k)]$.
According to [28], the overall system energy efficiency (EE) can be expressed as

$$\mathrm{EE} = \frac{B\sum_{k=1}^K R_k}{P^{\mathsf{total}}}, \tag{8}$$

where B represents the system bandwidth, and P^{total} is the total power consumption in the fully connected HBF architecture. Specifically,

$$P^{\mathsf{total}}(\boldsymbol{B}) = \xi\|\boldsymbol{B}\|_F^2 + P_{\mathsf{t}}, \tag{9}$$

$$P_{\mathsf{t}} = N_{\mathsf{t}}M_{\mathsf{t}}P_{\mathsf{PS}}(b) + M_{\mathsf{t}}P_{\mathsf{RFC}} + P_{\mathsf{LO}} + P_{\mathsf{BB}}, \tag{10}$$

$$P_{\mathsf{RFC}} = P_{\mathsf{DAC}} + P_{\mathsf{mixer}} + P_{\mathsf{LPF}} + P_{\mathsf{BBA}}, \tag{11}$$

where ξ is the inverse of the amplifier efficiency, $P_{\mathsf{PS}}(b)$, P_{RFC}, P_{LO} and P_{BB} represent the power consumption of phase shifter (depending on the bit resolution b), RF, local oscillator and baseband beamforming respectively. Additionally, $\boldsymbol{B} \triangleq (\boldsymbol{b}_1, \ldots, \boldsymbol{b}_K)$. The power consumption of the RF device consists of four parts: digital-to-analog converter, mixer, low-pass filter and baseband amplifier, which are represented by P_{DAC}, P_{mixer}, P_{LPF} and P_{BBA} respectively. Since the total power consumption for a fully digital architecture is

$$P_{\text{t-DBF}} = N_{\mathsf{t}}P_{\mathsf{RFC}} + P_{\mathsf{LO}} + P_{\mathsf{BB}}, \tag{12}$$

the optimization problem considered consists of maximizing the EE with discrete phase constraints:

$$\begin{aligned}\mathcal{P}_1 : \underset{\boldsymbol{V},\boldsymbol{W}}{\text{maximize}} \quad & \frac{B\sum_{k=1}^K R_k}{P^{\mathsf{total}}(\boldsymbol{V}\boldsymbol{W})} \\ \text{s.t. } & \|\boldsymbol{V}\boldsymbol{W}\|_F^2 \leq P, \qquad \boldsymbol{V} \in \mathcal{S}_b^{N_{\mathsf{t}}\times M_{\mathsf{t}}}.\end{aligned} \tag{13}$$

In the fully-digital case ($b \to \infty$), the last constraint is omitted:

$$\mathcal{P}_1' : \max_{\boldsymbol{B}} \frac{B\sum_{k=1}^K R_k}{P^{\mathsf{total}}(\boldsymbol{B})} \quad \text{s.t.} \quad \|\boldsymbol{B}\|_F^2 \leq P. \tag{14}$$

III. Optimization algorithm

The optimization framework proposed in this work is divided in two steps:

- Fully Digital Beamforming optimization consisting of determining the beamforming matrix maximizing an upper bound on the average user rate by using the Quadratic Transform method [29].
- Alternating and Manifold Based Hybrid Analog-Digital Beamforming consisting in the optimum approximation of the beamforming matrix as the product of its analog and digital parts.

A. Fully Digital Beamforming

To solve the energy-efficiency optimization problem in a LEO single-satellite system, an equivalent fully digital beamforming approach is first presented. The key idea is to consider a unified digital beamformer, allowing the problem to be reformulated using an upper bound on the average user rate. By leveraging this upper bound and applying the Quadratic Transform (QT) method [29], the non-convex energy efficiency maximization problem is transformed into an iterative optimization framework. Each iteration involves updating auxiliary variables and solving a constrained optimization problem via Lagrangian duality.

Due to the high orbital speeds of LEO satellites, it is essential to compute beamforming coefficients rapidly. To address this challenge, we developed an efficient beamforming solution that leverages the Woodbury matrix identity, significantly reducing the computational complexity of matrix inversion. A detailed description of the optimization algorithm is reported in [30].

B. Alternating and Manifold Based Hybrid Analog-Digital Beamforming

A hybrid beamforming approach that approximates the fully digital solution using the minimum Euclidean distance criterion is proposed. The core problem is approached as a least-squares optimization to minimize the difference between the digital beamformer and the product of analog and digital hybrid beamformers. The resulting algorithm alternates between the following steps:

- **Digital beamformer update**: Solved in closed form using the pseudo-inverse of the fixed analog beamformer.
- **Analog beamformer update**: Formulated as a constrained optimization problem on a complex oblique manifold to satisfy constant-modulus constraints.

To solve the non-convex analog subproblem, *manifold optimization* is used. A Riemannian gradient is computed by projecting the Euclidean gradient onto the manifold's tangent space. Then, an Armijo backtracking line search determines the step size, and a retraction step ensures compliance with hardware-imposed phase quantization. Since initialization of the analog beamformer significantly affects convergence, random initialization is used to avoid getting stuck in poor local optima. The results obtained by this approach are better than

TABLE I
SIMULATION PARAMETERS

Parameter	Value
Phased array	Square array
Number of full array elements	64
Element spacing	0.5λ
Center frequency	1.9 GHz
Total n. of users	8
β_k	18 dB
System bandwidth B	20 MHz
ξ	2

TABLE II
POWER PARAMETERS

Parameter	Value (mW)
P_{DAC}	400
P_{mixer}	15
P_{LPF}	10
P_{BBA}	5
P_{LO}	5
P_{BB}	200
$P_{\mathsf{PS}}(2), P_{\mathsf{PS}}(3), P_{\mathsf{PS}}(4), P_{\mathsf{PS}}(\infty)$	12,18,24,30

using deterministic schemes like Maximum Ratio Transmission (MRT). The complete algorithm iteratively updates analog and digital matrices until convergence. Manifold optimization ensures constraint satisfaction and improved performance under hardware limitations. A complete description is reported in [30].

IV. SIMULATION RESULTS

A near-hexagonal planar array with half-wavelength spacing is assumed, with coherent combining user antennas. Simulation parameters are listed in Table I (see [8]). The large-scale downlink channel power gain for the k-th user terminal (UT) is given by

$$\gamma_k = G_{\text{s}} G_{\text{u}} N_{\text{t}} \left(\frac{v_{\text{c}}}{4\pi f_{\text{c}} d_k} \right)^2, \quad \forall\, k \in \{1, \ldots, K\}, \qquad (15)$$

where G_{s} and G_{u} are the satellite and ground antenna gains, f_{c} the carrier frequency, v_{c} the speed of light, and d_k the distance between the k-th UT and the LEO satellite. The antenna gain is modeled according to the ITU-R S.1528 specifications [26] and the power consumption settings are shown in Table II [31, 32].

Fig. 4 describes the EE versus the number of RF chains with different phase shifter resolutions based on the AMHB algorithm and $P = 10$ dBW. With the fully connected HBF architecture, the smaller the number of RF chains, the greater the corresponding EE. However, as the resolution increases, the EE decreases because the higher resolution of the phase shifter increases the power consumption. When the number of RF chains is equal to the number of users, the EE performance of the fully connected HBF structure is better than that of the DBF structure. Therefore, the use of a fully connected HBF architecture with a limited number of RF chains can effectively reduce hardware complexity while improving the

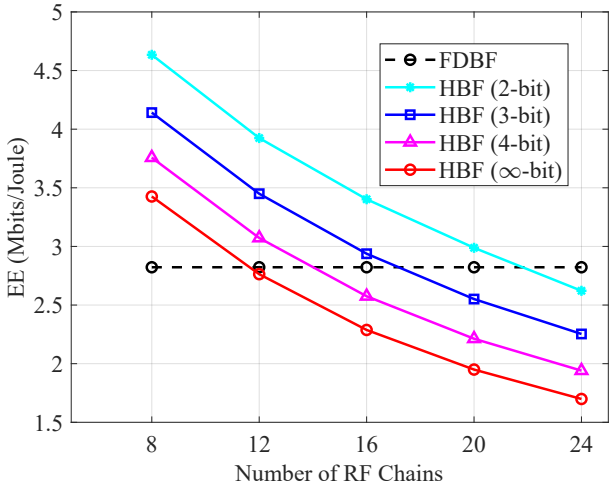

Fig. 4. Plot of the EE versus the number of RF chains with different resolutions and $P = 10$ dBW.

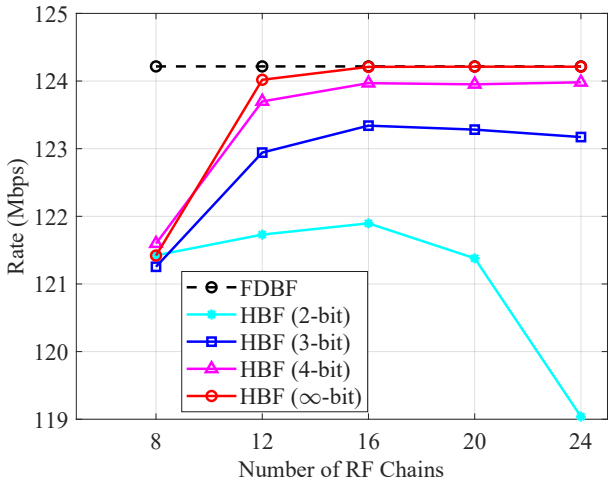

Fig. 5. Plot of the sum rate versus the number of RF chains with different resolutions and $P = 10$ dBW.

EE performance. Fig. 5 illustrates the sum rate versus the total number of RF chains. As the resolution increases, the sum rate increases, too, but saturates at 4 bits. The diagrams show an optimum number of RF chains $M_t \approx 16$ in the scenario considered. Fig. 6 shows the EE vs. the power budget for different phase resolutions with 8 RF chains. Solid lines use the AMHB algorithm and the dashed line uses the ideal DBF with infinite resolution. The EE peaks near $P = 6$ dBW for HBF with 2-bit resolution and saturates beyond that due to a transmission power threshold in LEO satellites. Fully connected HBF outperforms DBF in EE under infinite resolution by reducing the RF chain count and trading slight spectral efficiency loss for lower power consumption. Finally, in Fig. 7, the Hybrid Design by Fast Unitary Matching (HD-FUM) [33] and the Accelerate Proximal Gradient (APG) [34] algorithms are compared with our proposed AMHB algorithm. It can be seen that the proposed algorithm has better EE performance under the fully connected HBF architecture in both finite

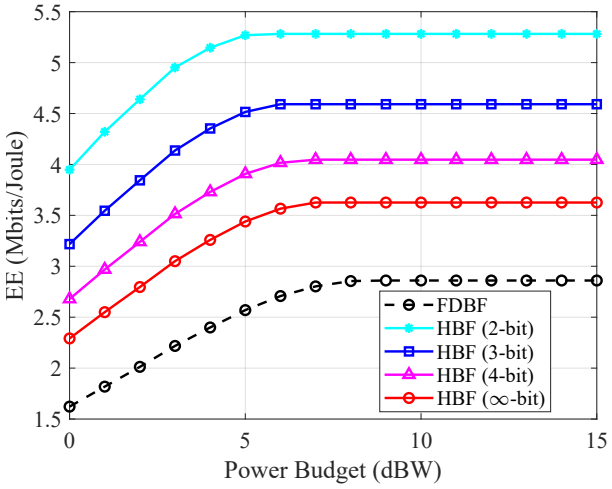

Fig. 6. Plot of the EE with 8 RF chains and different resolutions versus the power budget P.

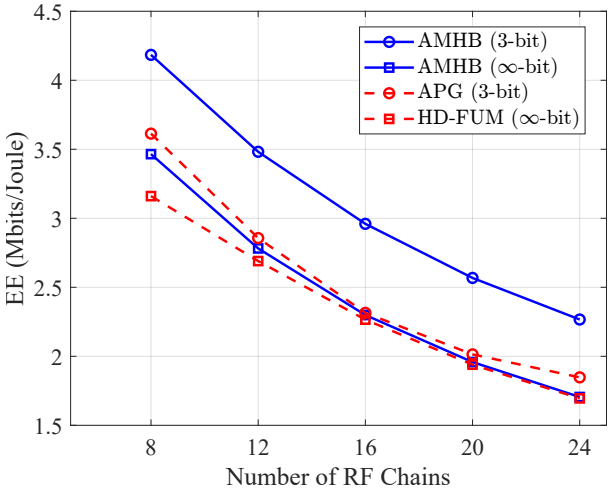

Fig. 7. Plot of the EE versus the number of RF chains with different HBF algorithms.

resolution and infinite resolution, and the gain is greater with fewer RF links.

V. Conclusions

In this paper, we investigated a downlink transmission framework for a single LEO satellite system using a fully connected hybrid analog–digital beamforming (HBF) architecture. Our work focuses on the enhancement of the energy efficiency under realistic hardware constraints, such as finite-resolution phase shifters and limited power amplifier capabilities. An equivalent fully digital beamforming solution was derived by using fractional programming and the QT algorithm to provide a performance upper bound. Building upon this foundation, we proposed an alternating and manifold based hybrid analog-digital beamforming (AMHB) algorithm that efficiently approximates the fully digital solution with substantially fewer RF chains. Numerical results show that the proposed AMHB algorithm significantly reduces system power consumption and improves energy efficiency under the premise of small system sum rate loss. The effect is more obvious for HBF structures with fewer RF numbers.

References

[1] L. Lei, A. Wang, E. Lagunas, X. Hu, Z. Zhang, Z. Wei, and S. Chatzinotas, "Spatial–temporal resource optimization for uneven-traffic LEO satellite systems: Beam pattern selection and user scheduling," *IEEE Journal on Selected Areas in Communications*, vol. 42, no. 5, pp. 1279–1291, May 2024.

[2] J. Li, G. Sun, Q. Wu, D. Niyato, J. Kang, A. Jamalipour, and V. C. M. Leung, "Collaborative ground-space communications via evolutionary multi-objective deep reinforcement learning," *IEEE Journal on Selected Areas in Communications*, vol. 42, no. 12, pp. 3395–3411, Dec 2024.

[3] Y. Zhu, L. You, Q. Kong, G. Seco-Granados, and X. Gao, "Robust precoding for massive MIMO LEO satellite localization systems," *IEEE Transactions on Vehicular Technology*, vol. 74, no. 2, pp. 3434–3438, Feb 2025.

[4] X. Lin, S. Cioni, G. Charbit, N. Chuberre, S. Hellsten, and J.-F. Boutillon, "On the path to 6G: Embracing the next wave of low earth orbit satellite access," *IEEE Communications Magazine*, vol. 59, no. 12, pp. 36–42, December 2021.

[5] K. Ntontin, E. Lagunas, J. Querol, J. u. Rehman, J. Grotz, S. Chatzinotas, and B. Ottersten, "A vision, survey, and roadmap toward space communications in the 6G and beyond era," *Proceedings of the IEEE*, pp. 1–37, 2025.

[6] H. Zhang, H. Zhao, R. Liu, X. Gao, and S. Xu, "Dynamic user association and computation offloading in satellite edge computing networks via deep reinforcement learning," *IEEE Transactions on Green Communications and Networking*, vol. 8, no. 4, pp. 1888–1901, Dec 2024.

[7] B. Al Homssi, A. Al-Hourani, K. Wang, P. Conder, S. Kandeepan, J. Choi, B. Allen, and B. Moores, "Next generation mega satellite networks for access equality: Opportunities, challenges, and performance," *IEEE Communications Magazine*, vol. 60, no. 4, pp. 18–24, April 2022.

[8] L. You, K.-X. Li, J. Wang, X. Gao, X.-G. Xia, and B. Ottersten, "Massive MIMO transmission for LEO satellite communications," *IEEE Journal on Selected Areas in Communications*, vol. 38, no. 8, pp. 1851–1865, Aug 2020.

[9] C. Lu, J. Shi, B. Li, and X. Chen, "Dynamic resource allocation for low earth orbit satellite networks," *Physical Communication*, vol. 67, p. 102498, 2024.

[10] C. Fulton, M. Yeary, D. Thompson, J. Lake, and A. Mitchell, "Digital phased arrays: Challenges and opportunities," *Proceedings of the IEEE*, vol. 104, no. 3, pp. 487–503, March 2016.

[11] Y. Zhang, Q. Cui, W. Ni, and P. Zhang, "Energy-efficient transmission of hybrid array with non-ideal power amplifiers and circuitry," *IEEE Transactions on Wireless*

Communications, vol. 17, no. 6, pp. 3945–3958, June 2018.

[12] M. Alsenwi, E. Lagunas, and S. Chatzinotas, "Robust beamforming for massive MIMO LEO satellite communications: A risk-aware learning framework," *IEEE Transactions on Vehicular Technology*, vol. 73, no. 5, pp. 6560–6571, May 2024.

[13] A. Alkhateeb, G. Leus, and R. W. Heath, "Limited feedback hybrid precoding for multi-user millimeter wave systems," *IEEE Transactions on Wireless Communications*, vol. 14, no. 11, pp. 6481–6494, Nov 2015.

[14] L. Wen, H. Qian, X. Luo, and K. Kang, "Hybrid beamforming design with finite resolution phase shifters in multi-user systems," in *2022 14th International Conference on Wireless Communications and Signal Processing (WCSP)*, Nov 2022, pp. 1007–1011.

[15] J. Jee, G. Kwon, and H. Park, "Precoding design and power control for SINR maximization of MISO system with nonlinear power amplifiers," *IEEE Transactions on Vehicular Technology*, vol. 69, no. 11, pp. 14 019–14 024, Nov 2020.

[16] O. E. Ayach, S. Rajagopal, S. Abu-Surra, Z. Pi, and R. W. Heath, "Spatially sparse precoding in millimeter wave MIMO systems," *IEEE Transactions on Wireless Communications*, vol. 13, no. 3, pp. 1499–1513, March 2014.

[17] H. Luyen, Z. Zhang, J. H. Booske, and N. Behdad, "Wideband, beam-steerable reflectarray antennas exploiting electronically reconfigurable polarization-rotating phase shifters," *IEEE Transactions on Antennas and Propagation*, vol. 70, no. 6, pp. 4414–4425, June 2022.

[18] J. Cong, T. Lin, and Y. Zhu, "Hybrid MMSE beamforming for multiuser millimeter-wave communication systems," *IEEE Communications Letters*, vol. 22, no. 11, pp. 2390–2393, Nov 2018.

[19] K. Y. Zhong, Y. J. Cheng, H. N. Yang, and B. Zheng, "LEO satellite multibeam coverage area division and beamforming method," *IEEE Antennas and Wireless Propagation Letters*, vol. 20, no. 11, pp. 2115–2119, Nov 2021.

[20] M. Y. Abdelsadek, G. K. Kurt, and H. Yanikomeroglu, "Distributed massive MIMO for LEO satellite networks," *IEEE Open Journal of the Communications Society*, vol. 3, pp. 2162–2177, 2022.

[21] Z. Lin, M. Lin, B. Champagne, W.-P. Zhu, and N. Al-Dhahir, "Secrecy-energy efficient hybrid beamforming for satellite-terrestrial integrated networks," *IEEE Transactions on Communications*, vol. 69, no. 9, pp. 6345–6360, Sep. 2021.

[22] F. Shao, H. Wang, C. Huang, G. Li, and W. Gong, "A novel phased array architecture with mixed-resolution phase shifters," *IEICE Transactions on Communications*, pp. 1–10, 2025.

[23] X. Fang, W. Feng, Y. Wang, Y. Chen, N. Ge, Z. Ding, and H. Zhu, "NOMA-based hybrid satellite-uav-terrestrial networks for 6G maritime coverage," *IEEE Transactions on Wireless Communications*, vol. 22, no. 1, pp. 138–152, Jan 2023.

[24] T. Shi, S. Sun, S. Kang, W. Sun, and R. Liu, "Robust multi-cast beamforming optimization on actual spectral efficiency in satellite systems," *IEEE Transactions on Vehicular Technology*, vol. 74, no. 1, pp. 1010–1019, Jan 2025.

[25] ITU-T, "TR-FG-NET2030 Sub-G1 (2020)," International Telecommunication Union, Technical Report, 2020.

[26] International Telecommunication Union (ITU), "Satellite Antenna Radiation Patterns for Non-Geostationary Orbit Satellite Antennas Operating in the Fixed-Satellite Service Below 30 GHz: ITU-R S.1528," International Telecommunication Union (ITU), Geneva, Tech. Rep. ITU-R S.1528, 2001.

[27] A. Adhikary, J. Nam, J.-Y. Ahn, and G. Caire, "Joint spatial division and multiplexing—the large-scale array regime," *IEEE Transactions on Information Theory*, vol. 59, no. 10, pp. 6441–6463, Oct 2013.

[28] C. G. Tsinos, S. Maleki, S. Chatzinotas, and B. Ottersten, "On the energy-efficiency of hybrid analog–digital transceivers for single- and multi-carrier large antenna array systems," *IEEE Journal on Selected Areas in Communications*, vol. 35, no. 9, pp. 1980–1995, Sep. 2017.

[29] K. Shen and W. Yu, "Fractional programming for communication systems—Part I: Power control and beamforming," *IEEE Transactions on Signal Processing*, vol. 66, no. 10, pp. 2616–2630, May 2018.

[30] D. Kong, G. Taricco, and Q. Guo, "Precoding algorithms for single-satellite LEO communication systems," *submitted for publication*, 2025.

[31] R. Méndez-Rial, C. Rusu, N. González-Prelcic, A. Alkhateeb, and R. W. Heath, "Hybrid mimo architectures for millimeter wave communications: Phase shifters or switches?" *IEEE Access*, vol. 4, pp. 247–267, 2016.

[32] C. Chen, Y. Dong, X. Cheng, and L. Yang, "Low-resolution PSs based hybrid precoding for multiuser communication systems," *IEEE Transactions on Vehicular Technology*, vol. 67, no. 7, pp. 6037–6047, July 2018.

[33] C. Rusu, R. Mènde z-Rial, N. González-Prelcic, and R. W. Heath, "Low complexity hybrid precoding strategies for millimeter wave communication systems," *IEEE Transactions on Wireless Communications*, vol. 15, no. 12, pp. 8380–8393, Dec 2016.

[34] X. Cui and Q. Li, "Hybrid beamforming with finite-resolution phase shifters for multiuser millimeter-wave downlink," *IEEE Wireless Communications Letters*, vol. 9, no. 2, pp. 219–222, Feb 2020.